JACS
JOURNAL OF THE AMERICAN CHEMICAL SOCIETY
Article
pubs.acs.org/JACS

Modulation of DNA Binding by Reversible Metal-Controlled Molecular Reorganizations of Scorpiand-like Ligands

Mario Inclán,[†] M. Teresa Albelda,*[,†] Juan C. Frías,[†,∥] Salvador Blasco,[†] Begoña Verdejo,[†] Carolina Serena,[‡] Clàudia Salat-Canela,[‡] Maria Luisa Díaz,[§] Antonio García-España,*[,‡] and Enrique García-España*[,†]

[†]Instituto de Ciencia Molecular, Departamento de Química Inorgánica, Universidad de Valencia, C/Catedrático José Beltrán 2, 46980 Paterna, Valencia, Spain

[‡]Unitat de Recerca, Hospital Joan XXIII, Institut de Investigació Sanitaria Pere Virgili (IISPV), Universitat Rovira i Virgili, C/Mallafré Guasch 4, 43007 Tarragona, Spain

[§]Pathology Department, Hospital Joan XXIII, Institut de Investigació Sanitaria Pere Virgili (IISPV), Universitat Rovira i Virgili, C/Mallafré Guasch 4, 43007 Tarragona, Spain

Supporting Information

ABSTRACT: DNA interaction with scorpiand azamacrocycles has been achieved through modulation of their binding affinities. Studies performed with different experimental techniques provided evidence that pH or metal-driven molecular reorganizations of these ligands regulate their ability to interact with calf thymus DNA (ctDNA) through an intercalative mode. Interestingly enough, metal-driven molecular reorganizations serve to increase or decrease the biological activities of these compounds significantly.

INTRODUCTION

The design of new small molecules that can interact with DNA[1] through recognition, binding, modification, cleavage, and cross-linking has been considered an attractive topic of research for many years.[2,3] Recognition of specific DNA sequences by a variety of molecules is fundamental to many biological processes, including transcription, replication, recombination, and chromosomal segregation during mitosis and meiosis. Similarly, other processes such as carcinogen- and radiation-induced DNA damage, repair of DNA lesions, and the mechanism of action of numerous anti-neoplastic agents involve specific ligand−DNA interactions. Moreover, DNA is generally the primary intracellular target of anticancer drugs,[4] so it is very important to obtain a better understanding different modes of drug binding to DNA for the consequent development of new, efficient DNA-targeted drugs with robust therapeutic profiles. In addition, knowledge of the chemical interactions that occur between small molecules and DNA is important for predicting the physiological potential and/or therapeutic effects of such interactions.

The binding modes that characterize the interactions of small molecules with double-stranded DNA are intercalation, groove binding, and covalent binding.[5] It should be noted that a single compound may use more than one mode of DNA molecular recognition and binding. As a consequence of these interactions, the structural changes induced in DNA by small molecules result in a disruption of the replication and transcription events, ultimately leading to apoptosis and cell death.[6] Many of the anticancer chemotherapeutic drugs find their basis of action in intercalative processes.[7] In this regard, current research efforts are still being directed toward the synthesis of new intercalative compounds with the ability to modulate their affinity to DNA.

Among the vast variety of molecules capable of binding to DNA, macrocyclic polyamines, which have a strongly basic nature, are known to be minor-groove binders as well as to interact electrostatically with the phosphates in the DNA or RNA backbone.[8] In an attempt to incorporate an intercalative functionality into the macrocyclic cavity in the hope of increasing the specificity and affinity toward DNA, we designed novel compounds **L1**, **L2**, and **L3** (Scheme 1).

Scorpiand-like ligands,[9] which consist of a "fixed" macrocyclic core appended with an arm containing additional donor groups, have the possibility to perform pH- or metal-driven molecular motions between extended and closed conformations depending on the pH of the medium and the presence of metal ions, as previously proved for **L5**, a ligand similar to **L1** but having a naphthalene moiety in place of the anthracene ring.[10] In addition, the presence of either an anthracene or a pyrene moiety in the scorpiand tail allows the use of fluorescence spectroscopy to signal the motions.

Since several literature references indicate that molecular reorganizations in ligands brought about by metal or other

Received: January 17, 2012
Published: May 17, 2012

Scheme 1

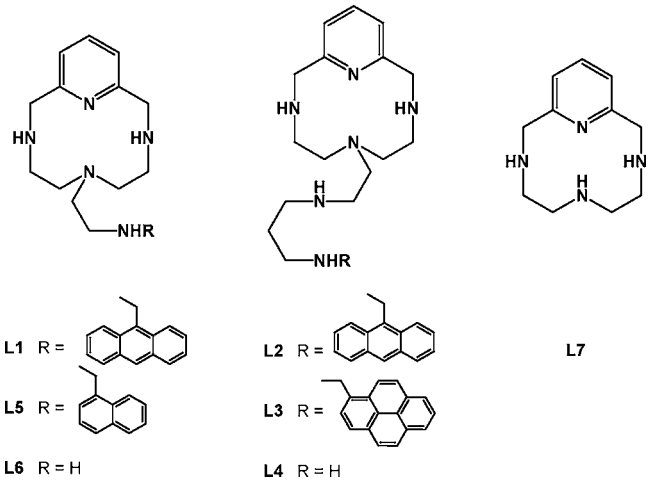

substrate binding could affect DNA interactions,[11] we thought that our compounds could be good candidates for exploring modulations of metal−DNA binding. To check this point, we first studied the protonation behavior and Cu^{2+} and Zn^{2+} metal complex formation of **L1**−**L3** in water. We then employed a variety of different techniques to analyze the interactions of **L1**−**L3** and of their Cu^{2+} and Zn^{2+} metal complexes with naked calf thymus DNA (ctDNA). Finally, we checked the in vitro cellular activity of **L1**−**L3** in the presence or absence of metal ions in cellular cultures of human bladder cancer cell lines.

RESULTS

Molecular Movements. *pH-Driven Molecular Reorganizations.* Table 1 collects the stepwise protonation constants of ligands **L1**−**L3** determined at 298.1 ± 0.1 K in 0.15 mol dm^{-3} NaCl. Ligand **L1** with only one donor atom in the tail presents three stepwise protonation constants in the pH range studied (2.5−11.0) that are separated by ca. 1.1 and 1.5 logarithmic units. It was not possible to measure a fourth protonation constant by pH-metric titration. This last protonation step should involve either the pyridine nitrogen atom or the central tertiary amino nitrogen of the macrocyclic ring. While protonation at the pyridine nitrogen in the 2.0−11.0 pH range of study is very unlikely in view of the literature precedents for analogous ligands,[10] protonation at the tertiary nitrogen should also have a very low value of the protonation constant, since this process would result in electrostatic repulsion with three charged polyammonium groups. On the other hand, it is well-known that tertiary nitrogen atoms are less basic in aqueous solution than primary and secondary ones, and this will contribute even more to the reduction in the basicity of this group.[12−14]

Table 1. Stepwise and Cumulative Protonation Constants for L1−L3 at 298.1 ± 0.1 K[a]

reaction[b]	L1	L2	L3
$L + H \rightleftarrows HL$	9.80(2)	10.09(1)	9.43(2)
$HL + H \rightleftarrows H_2L$	8.66(2)	9.31(1)	9.18(2)
$H_2L + H \rightleftarrows H_3L$	7.19(3)	8.03(3)	7.88(3)
$H_3L + H \rightleftarrows H_4L$	–	7.01(4)	6.92(3)
log β[c]	25.65(3)	34.44(1)	33.41(3)

[a]Logarithms of the stepwise (K_{H_jL}) and cumulative (β) protonation constants are reported. Values were determined in 0.15 mol dm^{-3} NaCl. Numbers in parentheses are standard deviations in the last significant figure. [b]Charges have been omitted. [c]Calculated as log $\beta = \sum_j \log K_{H_jL}$.

The existence of an additional donor atom in the tail (**L2** and **L3**) confers a fourth protonation step. Again, as described above for **L1**, it was not possible to calculate by potentiometry the constant for the protonation step involving the tertiary amino group in either of these ligands.

While the anthracene and pyrene absorption bands of **L1**−**L3** do not change significantly with pH, the fluorescence emission of **L1**−**L3** is quenched as the degree of protonation of the ligand decreases (Figure 1). This phenomenon has been widely observed in similar compounds and is attributed to a photoinduced electron transfer (PET) process from the lone pairs of the amine to the excited aromatic unit.[15]

A representation of the fluorescence emission titration curve conjointly with the mole fraction distribution curves for the differently protonated species (obtained by potentiometry) can be used to calculate the relative fluorescence emission of all the emissive species. Figure 2 shows as an example the case of **L1**, in which the largest fluorescence emission intensity occurs for the fully protonated form, with the first deprotonation resulting in a sharp decrease in the emission. Fluorescence emission titration curves for **L2** and **L3** are shown in Figure S1 in the Supporting Information.

The attachment of a flexible coordinating side chain to a rigid macrocycle generates some interesting properties. As mentioned above, we previously proved that the related ligand **L5** (Scheme 1) can perform molecular rearrangements in which the pendant arm approaches or moves away from the macrocyclic core as a result of not only the presence of metal ions but also just a change in the protonation state of the ligand.[10] In the latter case, hydrogen bonding and $\pi-\pi$ stacking interactions would be the driving forces of the motion. Scheme 2 illustrates pH-driven molecular movements of **L1**.

We carried out several studies to assess whether such molecular rearrangements also occur for **L1**−**L3**. First, the ^{1}H NMR spectra recorded at various pH show that in going from pH 5 to pH 8, corresponding with the deprotonation of $[H_3\mathbf{L1}]^{3+}$ to give $[H_2\mathbf{L1}]^{2+}$, there is an upfield shift of all the aromatic signals of both the anthracene and pyridine moieties (Figure 3), indicating that $\pi-\pi$ stacking between them occurs. Therefore, after the first deprotonation, the pendant arm of **L1** approaches the macrocyclic core and the system appears to adopt a closed conformation.

The ^{1}H NMR spectra of **L2** at various pH provide similar conclusions. The upfield shift of both the anthracene and pyridine aromatic signals in going from pH 6.0 to pH 7.7, corresponding to the first deprotonation of the ligand ($[H_4\mathbf{L2}]^{4+}$ to $[H_3\mathbf{L2}]^{3+}$), supports the occurrence of stacking between them. However, this upfield shift becomes much more pronounced at pH 9, where **L2** has lost two protons (Figure S2 in the Supporting Information).

In the pH range where the stacking of the pyridine and anthracene moieties occurs, the band centered at 253 nm experiences a bathochromic effect and a decrease in intensity (hypochromism). As an example, we have presented in Figure 4 the UV spectra of **L2** at different pH values.

To demonstrate that the observed hypochromism and bathochromic shift can be ascribed to $\pi-\pi$ stacking of the pyridine and anthracene moieties, we carried out the same experiment with ligand **L4**, which is structurally similar to **L2**

dx.doi.org/10.1021/ja300538s | J. Am. Chem. Soc. 2012, 134, 9644−9656

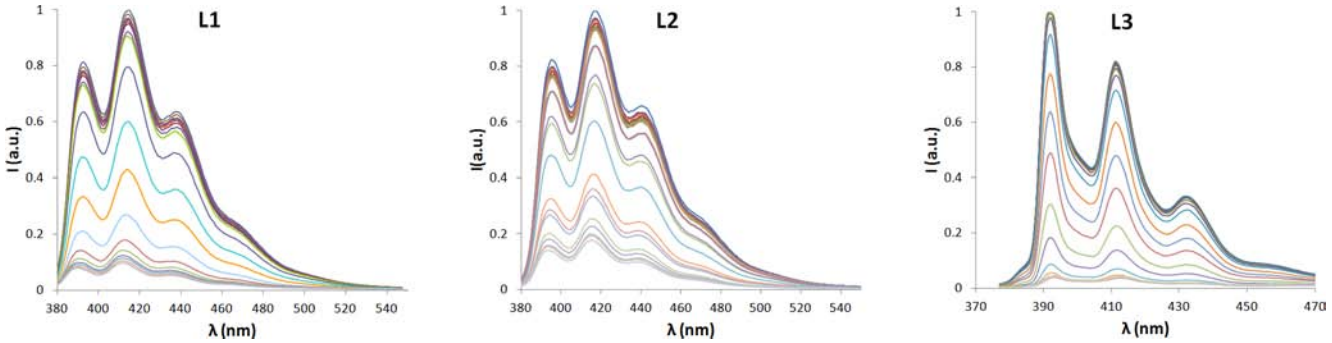

Figure 1. Fluorescence emission spectra of **L1** and **L2** (λ_{exc} = 365 nm) and **L3** (λ_{exc} = 346 nm) recorded at 298.1 ± 0.1 K in 0.15 mol dm^{-3} NaCl at pH ranging between 2 and 11 with [**L**] = 1.0 × 10^{-5} M.

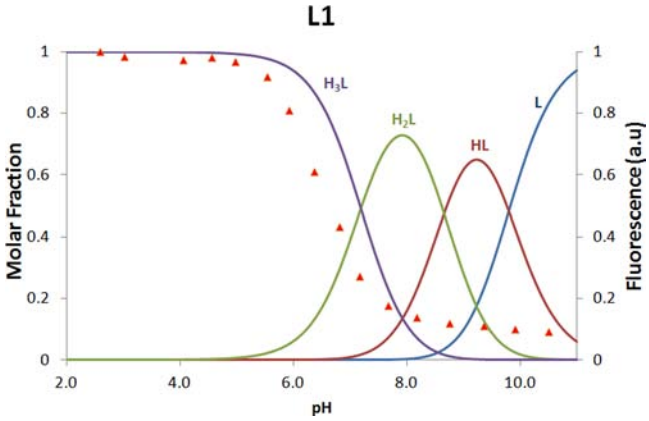

Figure 2. Steady-state fluorescence emission titration curve of **L1** (λ_{exc} = 365 nm) measured in 0.15 mol dm^{-3} NaCl at 298.1 ± 0.1 K with [**L**] = 1.0 × 10^{-5} M (red ▲) and mole fraction distribution curves for the various protonated forms (solid lines).

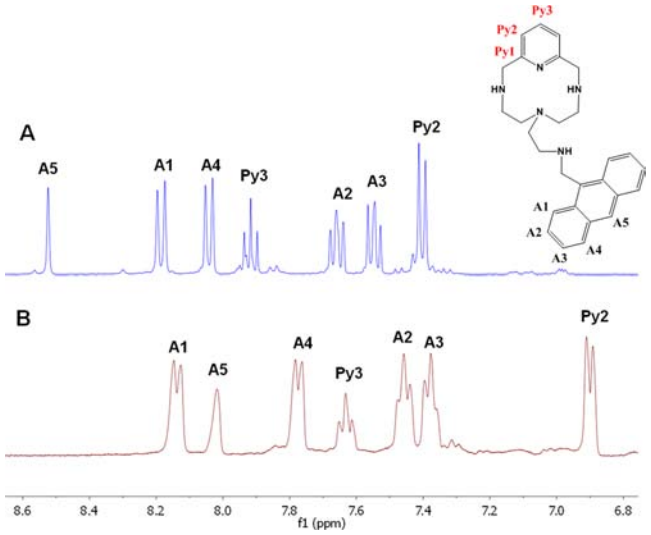

Figure 3. Aromatic signals of ^{1}H NMR spectra of **L1** in D_2O recorded at (A) pD 4.9 and (B) pD 8.0.

Scheme 2

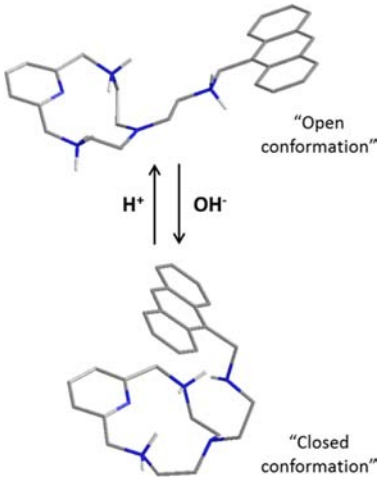

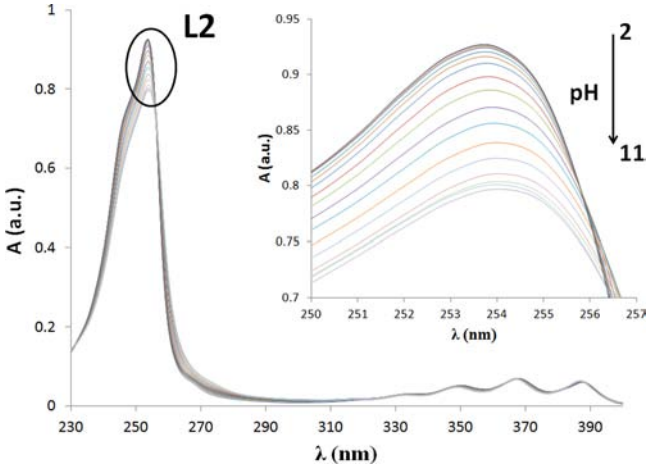

Figure 4. pH dependence of the absorption spectrum of **L2**.

but has not been functionalized with a chromophore in the pendant arm and therefore cannot display any intramolecular $\pi-\pi$ stacking. As shown in Figure 5, no hypochromism or bathochromic shift were observed; the only spectral change that occurred was a slight increase in the absorbance.

Using this UV−vis spectroscopic data, we calculated pK values of 6.75(1), 7.30(1), and 7.02(1) for **L1**, **L2**, and **L3**, respectively (Table 2). These values are in agreement with the results obtained by ^{1}H NMR spectroscopy and represent the mean values for which the motion of the tail takes place, switching from an open to a closed conformation of the ligand.

Metal-Induced Molecular Reorganizations. The use of metal ions as external input is another way to induce controllable molecular reorganizations. In this case, the macrocyclic ring encircles the metal and the flexible side chain (which contains additional donor atoms) folds to coordinate the metal. In particular, we studied the interaction

dx.doi.org/10.1021/ja300538s | J. Am. Chem. Soc. 2012, 134, 9644−9656

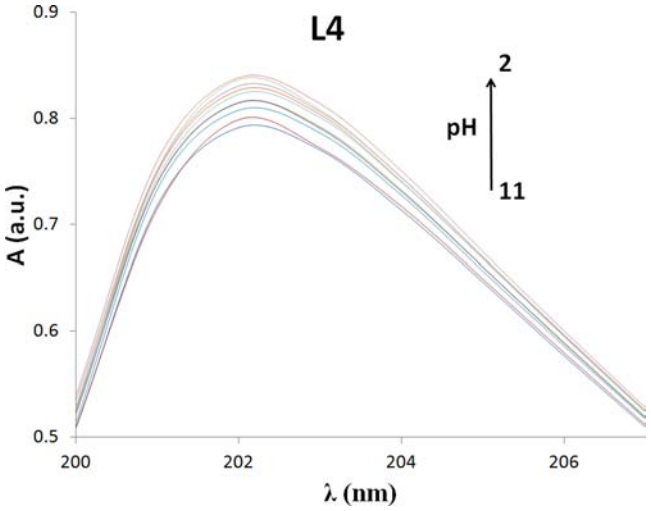

Figure 5. pH dependence of the absorption spectrum of **L4**.

Table 2. p*K* Values for pH- and Metal-Induced Conformational Changes in the Studied Ligands and Their Cu^{2+} and Zn^{2+} Complexes[a]

	free ligand	Cu^{2+} complex	Zn^{2+} complex
L1	6.75(1)	3.03(1)	4.62(1)
L2	7.30(1)	5.37(1)	6.00(4)
L3	7.02(1)	4.70(1)	6.30(1)

[a]Numbers in parentheses are standard deviations in the last significant figure.

of **L1**–**L3** with Cu^{2+} and Zn^{2+}, since it has been demonstrated that the coordination of metal ions with bioactive ligands can actually alter their binding modes toward nucleic acids.[16,17]

Table 3 gathers the stepwise and cumulative stability constants for the interactions of **L1**–**L3** with Cu^{2+} and Zn^{2+}

Table 3. Stepwise Stability and Protonation Constants for Cu^{2+} and Zn^{2+} Complexes of Scorpiands L1–L3 at 298.1 ± 0.1 K[a]

reaction[b]	L1	L2	L3
	Cu^{2+} Complexes		
L + Cu ⇄ CuL	18.48(1)	20.49(4)	20.09(5)
CuL + H ⇄ CuHL	3.94(1)	6.44(1)	6.19(3)
CuHL + H ⇄ CuH_2L	–	4.61(1)	4.30(3)
	Zn^{2+} Complexes		
L + Zn ⇄ ZnL	15.81(4)	17.8(1)	16.83(5)
ZnL + H ⇄ ZnHL	4.93(3)	7.42(4)	7.01(3)
ZnHL + H ⇄ ZnH_2L	–	4.93(3)	4.30(3)
ZnL + H_2O ⇄ ZnL(OH) + H	n.d.[c]	−10.3(2)	n.d.[c]

[a]Logarithms of the constants are reported. Values were determined in 0.15 mol dm^{-3} NaCl. Numbers in parentheses are standard deviations in the last significant figure. [b]Charges have been omitted. [c]Not detected.

determined at 298.1 ± 0.1 K in 0.15 mol dm^{-3} NaCl solutions. The formation of mononuclear complexes was detected for all of the ligands throughout the pH range studied, with **L1** displaying $[MHL]^{3+}$ and $[ML]^{2+}$ stoichiometries and **L2** and **L3** also exhibiting an additional $[MH_2L]^{4+}$ species. It is interesting to emphasize that the calculated stability constants are larger for those ligands with the longer pendant arm, indicating the participation of the second donor atom of the tail in the formation of the complex.

Figure 6 presents steady-state fluorescence emission titration curves for the Cu^{2+}–**L3** and Zn^{2+}–**L2** systems, and those for

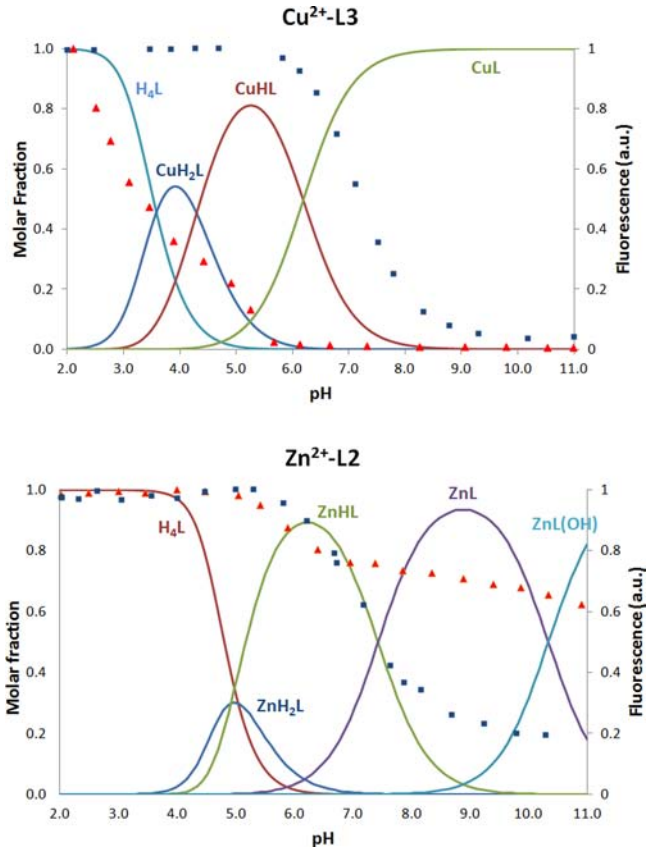

Figure 6. Steady-state fluorescence emission titration curves for (top) Cu^{2+}–**L3** and (bottom) Zn^{2+}–**L2** (red ▲) and the corresponding free ligands (blue ■) measured in 0.15 mol dm^{-3} NaCl at 298.1 ± 0.1 K with $[M^{2+}–L]$ or $[L] = 1.0 \times 10^{-5}$ M. The corresponding mole fraction distribution curves for H_4L and the various protonated forms of M^{2+}–**L** are shown as solid lines.

the Cu^{2+}–**L1**, Cu^{2+}–**L2**, and Zn^{2+}–**L3** systems are shown in Figure S3 in the Supporting Information. In the fluorescence emission studies of the Cu^{2+} complexes, a strong quenching effect was observed upon formation of the first complex species at acidic pH. In the titrations performed for a 1:1 M:**L** molar ratio, the quenching effect also was extended throughout all species at neutral and alkaline pH values. This quenching of the fluorescence emission upon Cu^{2+} complexation is commonly observed for polyamine ligands containing aromatic fluorophores and is attributed to energy-transfer quenching of the π^* emissive state through low-lying metal-centered states.[18]

Very different behavior was observed for the Zn^{2+} complexes, which showed an increase in the fluorescence relative to the free ligand (chelation-enhanced fluorescence). The PET does not take place when the ligands interact with Zn^{2+} because the nitrogen electrons are blocked through their participation in cation binding. The Zn^{2+}–**L1** complex was not studied at pH values higher than 6.5 because of solubility problems at basic pH.

Once again, this spectroscopic information was used to determine the p*K* value at which the open–closed rearrangement takes place. The p*K* values obtained for the complexes are

dx.doi.org/10.1021/ja300538s | *J. Am. Chem. Soc.* 2012, 134, 9644–9656

summarized in Table 2 along with those for the free ligands. It is worth noticing that the p*K* values for the metal complexes are smaller than those calculated for the free ligands, indicating that the presence of the metal cation forces the ligand to acquire the closed conformation, in which the donor atom located in the tail of the scorpiand ligand can coordinate the metal cation. As matter of fact, at pH 7, all of the metal complexes studied should essentially adopt the closed conformation.

Further confirmation of the geometry adopted by the complexes was obtained by X-ray diffraction of $[Cu(\mathbf{L1})](ClO_4)_2$ (Figure 7). The asymmetric unit contains four almost

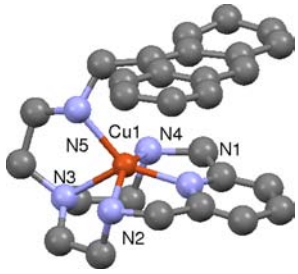

Figure 7. Ball-and-stick representation of the structure of the $[Cu(\mathbf{L1})]^{2+}$cation. H atoms have been omitted.

equivalent $[Cu(\mathbf{L1})]^{2+}$ cations and eight perchlorate counteranions. Although the solution of the crystal structure is rather bad because of the poor quality of the crystals and the thermal disorder associated with the perchlorate counteranions, it provides unambiguous indications about the closed conformation of the complex and the coordination sphere of the metal. In all of the $[Cu(\mathbf{L1})]^{2+}$ units, Cu^{2+} is coordinated by the four nitrogen atoms of the macrocycle and the secondary amino group of the pendant arm in a very slightly distorted square-pyramidal fashion ($\tau \approx 12\%$),[19] with the longest bond distance being that with the tertiary nitrogen of the macrocycle (2.12 Å; Table S2 in the Supporting Information). The pyridine and anthracene units are stacked at a distance of 3.6 Å. Therefore, it seems that in $[Cu(\mathbf{L1})](ClO_4)_2$ the stacking of the pyridine and anthracene rings somehow cancels the Jahn–Teller effect and prevents the axial position from being markedly distorted.

Since metal ion coordination is the driving force causing the tail to bend toward the macrocyclic core, such reorganization also occurs for the metal complexes of **L4**, the ligand without the intercalating unit. This is shown by the crystal structure of the complex $[Cu(\mathbf{L4})](ClO_4)_2$, shown in Figure 8. The metal is coordinated with a distorted octahedral geometry. The pyridine nitrogen, the tertiary nitrogen of the macrocyclic core, and the

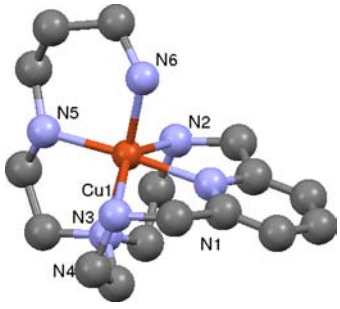

Figure 8. Ball-and-stick representation of the structure of the $[Cu(\mathbf{L4})]^{2+}$cation. H atoms have been omitted.

secondary and primary nitrogen atoms of the pendant arm define the equatorial plane, while the axial positions are occupied by the secondary nitrogen atoms of the macrocyclic core close to the pyridine ring [2.3363(1) and 2.3954(1) Å; Table S4 in the Supporting Information].

Metal-Induced Modulation of DNA Binding. *UV–Vis Spectroscopy.* On the basis of the above results, we next investigated how these metal ion-driven molecular reorganizations could control the binding affinity and selectivity of these ligands for naked DNA. The interactions of **L1**–**L3** with DNA were characterized through UV–vis spectroscopic titrations. Figure 9 shows absorption titration data for **L1** and its Cu^{2+} and Zn^{2+} complexes. Addition of ctDNA in small aliquots to a solution of **L1** resulted in a strong decrease in the absorption of the anthracene chromophore along with a red shift of 8 nm (Figure 9). The hypochromism was suggested to be due to strong interactions between the electronic states of the intercalating chromophore and those of the DNA base pairs. One isosbestic point was observed at 394 nm. The spectral changes shown in this figure (hypochromicity, red shift, and isosbestic point) are consistent with intercalation of the chromophore into the stacked DNA base pairs.[20,21] This mode of interaction has been well-described in the literature for other anthracene derivatives.[22]

Although similar spectral changes were observed for the copper and zinc complexes, the effect obtained in the case of the free ligand was larger. In the case of the zinc complex, almost no bathochromic shift was registered. As mentioned above, upon metal binding the ligand adopts a closed conformation that hinders its ability to interact with DNA.

Similar features were observed for **L2** and its Cu^{2+} and Zn^{2+} complexes (Figure S4 in the Supporting Information). However, although the hypochromicity observed for free **L2** was again greater than those for the copper and zinc complexes, the difference was not as important as the one described above for **L1** and its corresponding metal complexes. This behavior may be explained if we take into account the fact that at pH 7, the mole fraction of $[Cu(\mathbf{L1})]^{2+}$ is 100%, while for **L2** the mole fraction decreases to less than 80%, with the remaining 20% being the protonated species $[Cu(\mathbf{HL2})]^{3+}$, which we have previously determined to be in the open conformation.[23]

Finally, Figure S5 in the Supporting Information shows the absorption titration results for **L3** and its metal complexes. Again, large hypochromism followed by an 11 nm bathochromic shift were observed. These changes were greater than those presented by the anthracene-based ligands **L1** and **L2**. This suggests that the pyrene functionality may work better as an intercalator than the anthracene one.

UV–vis titration data were also used to estimate the binding constants of the ligands and complexes with ctDNA (Table 4). These values indicate the total interaction between the ligand/complex and DNA, including all modes of binding. All of the calculated stability constants are on the same order of magnitude (10^5 M^{-1}), indicating that all of the compounds use different modes of DNA molecular recognition and binding besides intercalation.

The changes in the absoption spectra of **L1**–**L3** after addition of DNA also indicated the presence of strong interactions between the chromophore and the base pairs of DNA. This hypochromism is observed when two chromophores are stacked one on top of the other.[24] Quantitatively expressed by the percent hypochromism, it can be used as a measure of the interaction (Figure 10). A first observation is

dx.doi.org/10.1021/ja300538s | *J. Am. Chem. Soc.* 2012, 134, 9644–9656

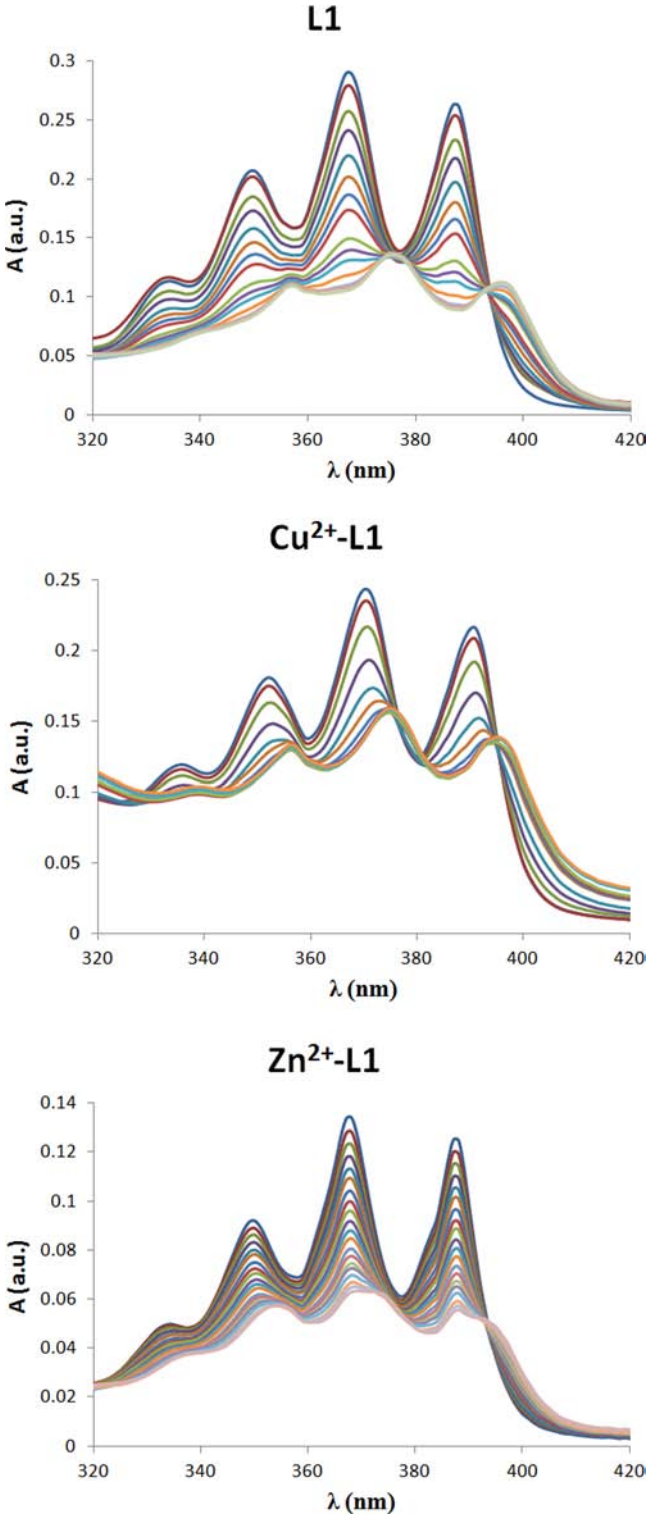

Figure 9. Absorption spectra of **L1** and M^{2+}–**L1** (50 μM) at pH 7 (50 mM sodium cacodylate buffer) with increasing ctDNA concentration (0–125 μM).

that all of the free ligands exhibit an important hypochromic effect, indicative of intermolecular interaction between anthracene/pyrene and the base. This hypochromic effect is larger than in the case of the metal complexes.

Steady-State Fluorescence Emission. Fluorescence titration experiments were also used to investigate the interactions of **L1**–**L3** with ctDNA. Addition of ctDNA to a solution of **L1** or

Table 4. Stability Constants Calculated from UV–Vis Titration Data for the Systems L/DNA and M^{2+}–L/DNA[a]

	free ligand	Cu^{2+}–L	Zn^{2+}–L
L1	5.04(3)	4.81(3)	3.86(1)
L2	4.69(4)	4.52(2)	4.06(1)
L3	–	4.35(1)	4.04(1)

[a]Logarithms of the stability constants are reported. Numbers in parentheses are standard deviations in the last significant figure.

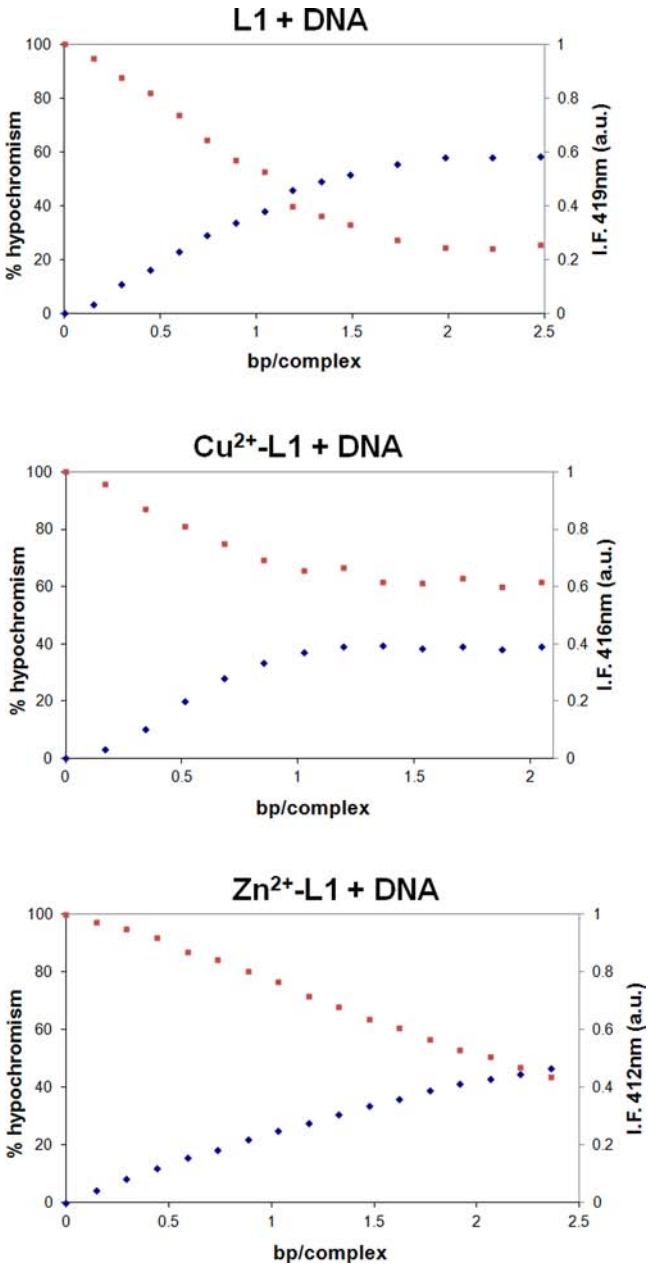

Figure 10. Plots of percent hypochromism (blue) and fluorescence intensity (red) vs base pair/complex ratio for **L1** and its Cu^{2+} and Zn^{2+} complexes upon addition of increasing amounts of ctDNA. (See Figures S6 and S7 in the Supporting Information for similar plots for **L2** and **L3**.)

$[M(\mathbf{L1})]^{2+}$ (M = Cu^{2+}, Zn^{2+}) resulted in strong fluorescence quenching. Although the use of fluorescence quenching to determine the mode of binding is clearly limited, the strong quenching obtained combined with the changes in the

dx.doi.org/10.1021/ja300538s | J. Am. Chem. Soc. 2012, 134, 9644–9656

absorption spectra suggest a preferential intercalative binding of these ligands with DNA (Figure 10 and Figures S6 and S7 in the Supporting Information).

Circular Dichroism. Further evidence for the strong interaction of the probes with the asymmetric environment of the DNA helix was provided by circular dichroism (CD) studies. In general, intercalators bound to the helix exhibit induced CD due to their asymmetric environment.[25] The CD spectra of **L1**−**L3** and their copper complexes were recorded in the presence of ctDNA (those for **L1** and $[Cu(\mathbf{L1})]^{2+}$ are shown in Figure 11 as an example, and the others are shown in Figure S8 in the Supporting Information). They display a distinct, strong decrease in the positive CD band at 280 nm and reveal the appearance of a new band at 260 nm. It is noteworthy that the induced CD peaks correspond to the absorption bands of the bound chromophore and not the free probe, consistent with the conclusion that the induced CD bands are due to the bound ligands and very likely originate from the intercalated chromophores.[26,27] It has to be remarked that in the case of $[Cu(\mathbf{L1})]^{2+}$, the band at 260 nm was not formed, confirming that the closed conformation of the complex is not well-suited for an intercalative binding mode.

In addition, we recorded the CD spectrum of **L4**, a scorpiand-like ligand that is not functionalized with an intercalative unit. As shown in the bottom panel of Figure 11, adding increasing amounts of this ligand to DNA did not cause any decrease in the CD band at 280 nm, and no induced CD bands were formed. This evidence proves that ligands **L1**−**L3** interact with DNA through the anthracene/pyrene aromatic moiety appended to the tail.

Thermal Denaturation. Table 5 shows the values obtained for the DNA melting temperatures (T_m) of 2:1 DNA/**L1**−**L3** mixtures. The effect of the copper complexes was also studied. The T_m of ctDNA alone was 78.4 °C. No major differences were found between the stabilization produced by each free ligand and its copper complex. The results clearly showed that compound **L3** has a stronger stabilization effect toward DNA than **L1** and **L2**. However, although it is known that intercalation of small molecules into the double helix typically increases T_m, the temperature at which the double helix denatures into single stranded DNA,[28] this method does not provide unambiguous evidence to distinguish intercalation from other binding modes.

Ethidium Bromide Displacement Studies. Further evidence for the intercalative mode of binding of these ligands was obtained from ethidium bromide (EB) displacement assays (Figure 12). Addition of any of the studied scorpiand-like ligands **L1**−**L3** resulted in a decrease in fluorescence due to the displacement of the bound EB intercalator, while practically no decrease was observed for **L4**, the compound without the appended chromophore unit, which was measured for comparative purposes. Since the percentage of the fluorescence decrease is directly related to the extent of binding, these experiments revealed that **L3** intercalates more effectively than **L2** or **L1**. Interestingly, assays performed with the Zn^{2+} complexes of **L1**−**L3** showed in all cases smaller EB displacements. When the experiment was carried out with the Zn^{2+} complex of **L4**, no significant differences with the results for uncomplexed **L4** were found.

Viscosity Measurements. Another simple and straightforward way to address the preferential binding mode of ligands with DNA is the measurement of viscosity. Intercalators dramatically increase the length of DNA, resulting in an

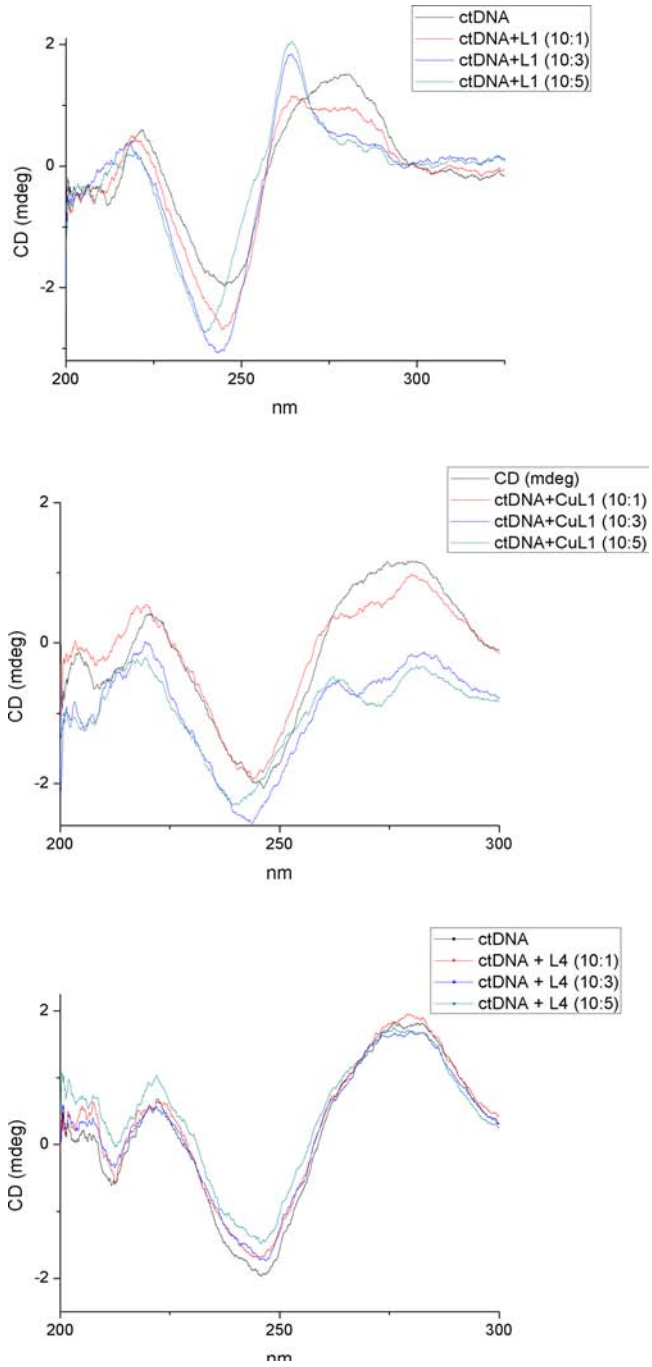

Figure 11. CD spectra of (top) **L1**, (middle) $[Cu(\mathbf{L1})]^{2+}$, and (bottom) ligand **L4** without the appended chromophore unit in the presence of ctDNA. The base/ligand mixing ratios were 10:1, 10:3, and 10:5; [ctDNA] = 30 μM in all of the spectra. (See Figure S8 in the Supporting Information for spectra for the other ligands.)

increased viscosity. In contrast, a groove binder does not lengthen the DNA helix and thus does not increase the viscosity of DNA solutions.[29] The viscosity measurements showed an increase in the viscosities of the DNA solutions upon addition of increasing amounts of **L1**−**L3**. For DNA interacting with the Zn^{2+} complexes, this behavior was reduced, showing again that the metal-induced conformational change affects the intercalating capacity of these ligands. The results for **L3**, Zn^{2+}−**L3**, and the unfunctionalized ligand **L4** (Figure 13) show how the presence of the metal affects the ligand behavior

dx.doi.org/10.1021/ja300538s | J. Am. Chem. Soc. 2012, 134, 9644−9656

Table 5. T_m and ΔT_m Values for ctDNA and ctDNA Interacting with L1−L3 and Their Copper Complexes[a]

compound	T_m (°C)	ΔT_m (°C)
ctDNA alone	78.4	–
ctDNA/**L1**	83.5	5.1
ctDNA/Cu^{2+}−**L1**	85.6	7.2
ctDNA/**L2**	89.1	10.7
ctDNA/Cu^{2+}−**L2**	88.5	10.1
ctDNA/**L3**	94.0	15.6
ctDNA/Cu^{2+}−**L3**	96.0	17.6

[a]The DNA/**L** ratio was 2:1 in all of the mixtures (50 mM sodium cacodylate buffer, pH 7).

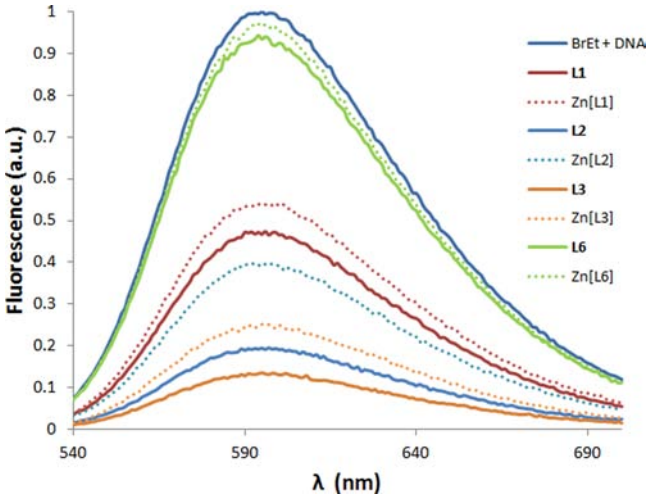

Figure 12. Fluorescence spectra obtained from EB displacement assays. The **L**/EB mixing ratio was 1:1; [EB] = [**L**] = 10 μM and [ctDNA] = 30 μM in all of the spectra. Top curve corresponds to EB + DNA alone. Other solid lines correspond to the free ligands and the dotted lines to the Zn^{2+} complexes.

and that **L4** behaves like a groove binder because of the absence of the aromatic chromophore.

Activity on Cancer Cell Lines. We next looked at the biological activity of **L1**−**L3** in cells, since DNA-intercalating molecules can inhibit nucleic acid synthesis and are being used

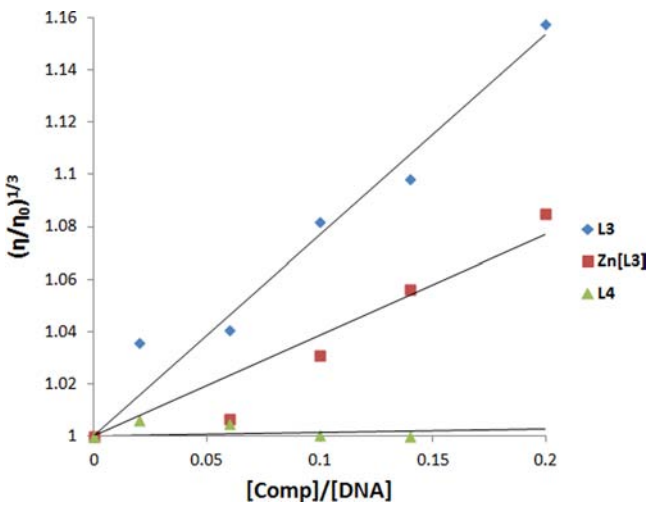

Figure 13. Relative viscosities of ctDNA in the presence of **L3** (blue), Zn^{2+}−**L3** (red), and **L4** (green).

as anticancer drugs. Also, as the above results indicate that metal ions induce conformational changes that influence **L1**−**L3** binding to naked DNA in solution, we analyzed whether, in living cells, metals could affect the biological activity of **L1**−**L3**. To do this, we used the MTT assay to assess cell viability in cultures of the human bladder cancer cell lines T24, 253J, and UMUC-3 (see the Experimental Section). These cancer cell lines have different combinations of mutations in tumor suppressor genes TP53 and retinoblastoma that could impinge on the degree of susceptibility to treatments with chemotherapeutic drugs.[30,31] To mimic as much as possible the in vivo cellular context, the cells were incubated with the compounds in whole-culture medium containing 10% serum.

Under these conditions, the uncoordinated **L1**−**L3** ligands were ∼20 times more cytotoxic than **L4**, **L6**, and **L7**,[10] which lack intercalating units, suggesting that the intercalating units of **L1**−**L3** mediate in part their cytotoxic effects in cells (Figure 14). While the half-maximal inhibitory concentrations (IC_{50}'s)

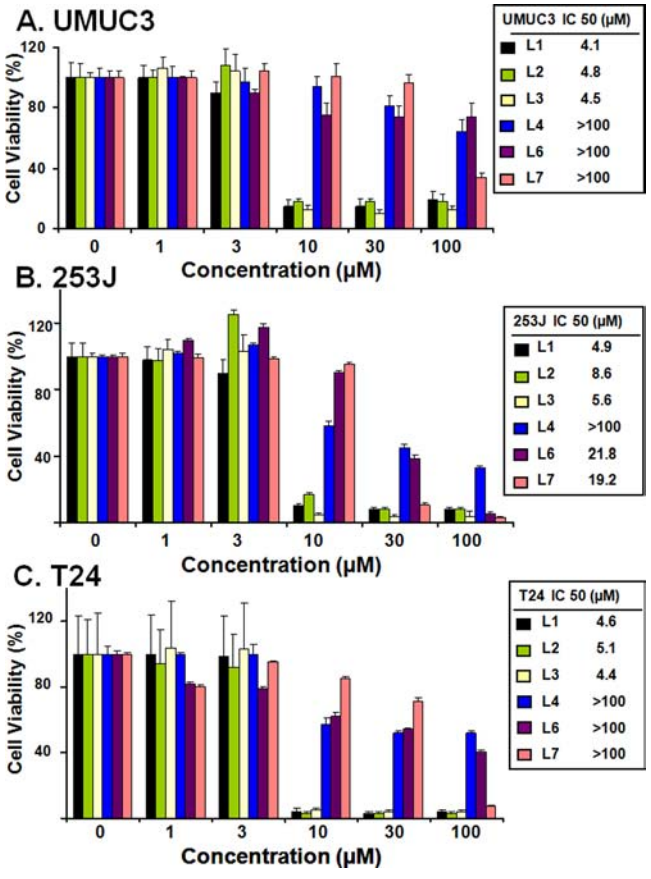

Figure 14. Cell viability reduction by uncoordinated **L1**−**L3** ligands. (A) UMUC-3, (B) 253J, and (C) T24 cells were treated for 48 h with 0, 1, 3, 10, 30, or 100 μmol L^{-1} uncoordinated ligand **L1** (black bars), **L2** (green bars), **L3** (yellow bars), **L4** (blue bars), **L6** (purple bars), or **L7** (pink bars). Cell viability is expressed as the percentage of the viability of untreated controls. Values are means ± standard errors for three independent experiments done in octuplicate.

for **L1**−**L3** were in the lower micromolar range, the IC_{50}'s for **L4**, **L6**, and **L7** were over 100 μM, except for **L6** and **L7** in 253J cells (see the insets in Figure 14).

When we compared the cytotoxicities elicited by uncoordinated **L1**−**L3** and the corresponding metal complexes, we observed that metal-complexed **L1**−**L3** were less cytotoxic. Cell

dx.doi.org/10.1021/ja300538s | J. Am. Chem. Soc. 2012, 134, 9644−9656

cytotoxicity was observable at concentrations over 3 μM for **L1**−**L3** (Figure 14) but not until concentrations over 100 μM for their metal complexes (Figure 15A and Figure S9 in the Supporting Information). Cells were almost 100% viable when incubated with metal-complexed **L1**−**L3** at 30 μM for 48 h, while they were less than 20% viable when incubated with the uncoordinated ligands, suggesting that the conformational change induced by the metal ions influences, at least in part, their cytotoxic effect on cells (Figure 15B). We used as controls **L7** and its metal complexes, since **L7** lacks pendant arms (Scheme 1). **L7** metal complexes were also less cytotoxic (Figure 15B), indicating that the metal ions could also hamper in part the cytotoxicity due to the nonintercalating parts of the compounds. Moreover, metal ions blocked the **L1**−**L3** cytotoxicity further when added on top of a culture medium of cells that had been already treated for 24 h with uncoordinated **L1**−**L3** ligands (Figure 15C).

In addition, taking advantage of the intrinsic fluorescence of **L2**, we were able to associate the presence of **L2** and Zn^{2+}−**L2** with individual living cells by fluorescence microscopy (Figure S10 in the Supporting Information). We observed **L2** fluorescence associated with living cells at 5 μM. We also noticed Zn^{2+}−**L2** fluorescence in living cells at 10 μM, while at this concentration of 10 μM, the cells treated with the uncoordinated **L2** had already died and detached from the plate, and only fluorescence associated with cell debris remained (Figure S10 in the Supporting Information).

Finally, we checked for the presence of DNA damage by looking at the activation of the cellular DNA damage response. Cellular DNA damage activates the ATM kinase, which in turn phosphorylates p53 protein at the Ser15 residue.[32] We used as positive controls doxorubicin and 5-fluorouracil, two anticancer drugs that are well-known activators of the DNA damage response (Figure 15D).[33] We observed that uncoordinated ligand **L2** but not its Zn^{2+} metal complex induced the cellular DNA damage response, as indicated by an increase in phosphorylation of the Ser15 residue of the p53 protein. Ser15 phosphorylation was enhanced in cells treated with uncoordinated **L2** in comparison with Zn^{2+}−**L2**-treated cells, indicating an interaction of the uncoordinated compound with DNA in living cells (Figure 15D).

The above results suggest that the interaction of the metal ions with the **L1**−**L3** ligands and the concomitant change in the ligand structure modulates, at least in part, their cytotoxic effects on cells.

■ CONCLUSIONS

The interactions between DNA and each of three synthesized scorpiand-like ligands containing appended anthracene and pyrene units were investigated by a variety of techniques. The results suggest that these compounds bind DNA efficiently through an intercalative mode. The presence or absence of Cu^{2+} or Zn^{2+} ions induces molecular reorganizations that change the ligand conformation from an open to a closed form, modulating the affinity of these systems for DNA. Interestingly enough, this is translated into a very significant increase in cell viability when the ligands are bound to a metal cation, allowing us to modulate the biological activity of these compounds. Further studies are currently being performed to introduce new regulation inputs in these and related ligands of this family.

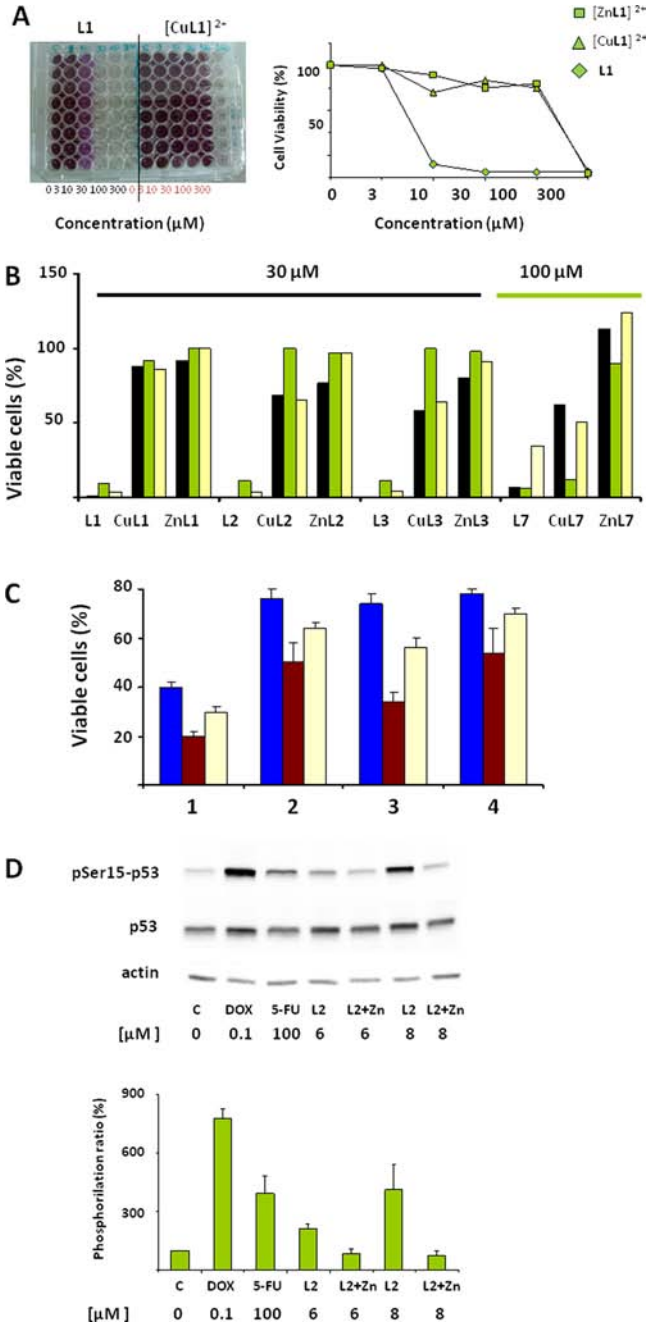

Figure 15. Coordination of Cu^{2+} and Zn^{2+} with ligands **L1**−**L3** prevents the reduction in cell viability. (A) Photograph of a 96-well culture plate of T24 cells after treatment with 0−300 μmol L^{-1} uncoordinated **L1** or the $[Cu(\mathbf{L1})]^{2+}$ complex (left panel). Corresponding cell viability graph including the treatment with $[Zn(\mathbf{L1})]^{2+}$ (right panel). (B) Cell lines T24 (black bars), 253J (green bars), and UMUC-3 (yellow bars) were treated for 48 h with 30 μmol L^{-1} **L1**−**L3**, 100 μmol L^{-1} **L7**, or their respective Cu^{2+} or Zn^{2+} complexes at the same concentrations. Results are plotted as the percentage of the viability of untreated cells. (C) Viability of T24 cells (1) after incubation with 8 μmol L^{-1} **L1** (blue bars), **L2** (brown bars), or **L3** (yellow bars) for 48 h; (2, 3) after incubation for 24 h with **L1**−**L3**, addition of 20 μL of 10 μmol L^{-1} $Cu(ClO_4)_2$ (2) or $Zn(ClO_4)_2$ (3) to the incubating medium, and further incubation for 24 h; or (4) after 24 h of incubation with **L1**−**L3**, replacement of the medium containing **L1**−**L3** with ligand-free medium, and further incubation for 24 h. Cell viability is expressed as the percentage of the viability of untreated controls after 48 h. (D) **L2** but not its Zn^{2+} complex activates the DNA damage response. Upper panel: representative

dx.doi.org/10.1021/ja300538s | J. Am. Chem. Soc. 2012, 134, 9644−9656

Figure 15. continued

Western blot of UMUC-3 cells incubated for 16 h with 6 or 8 μmol L^{-1} **L2** or its metal complexes. Doxorubicin (Dox) and 5-fluorouracil (5-FU) were used as controls. Lower panel: Phosphorylation fold increase (calculated as the ratio of pSer15-p53/p53 protein expression) plotted as the percentage of the control for each Western blot.

EXPERIMENTAL SECTION

Synthesis. All reagents and chemicals were obtained from commercial sources and used as received. Solvents used for the chemical synthesis were of laboratory or analytical grade and used without further purification.

*6-(2-Aminoethyl)-3,6,9-triaza-1-(2,6)-pyridinecyclodecaphane (**L6**).* This scorpiand ligand was conveniently used as a precursor in the synthesis of **L1**. It was prepared following the synthetic strategy reported in ref 10.

*6-[4-(9-Anthryl)-3-azabutyl]-3,6,9-triaza-1-(2,6)-pyridinecyclodecaphane (**L1**).* **L6** (0.84 g, 3.4 mmol) was dissolved in dry ethanol (150 mL), and a solution of 100 mL of dry ethanol containing anthracene-9-carboxaldehyde (0.9 g, 4.4 mmol) was added dropwise. The mixture was then stirred for 2 h. $NaBH_4$ (1.27 g, 34 mmol) was added, and the resulting solution was stirred for 1 h at room temperature. The solvent was evaporated under reduced pressure, and the resulting residue was treated with H_2O. The product was repeatedly extracted with dichloromethane (3 × 30 mL). The organic phase was dried (Na_2SO_4) and evaporated to yield the free amine, which was dissolved in ethanol and precipitated as the hydrochloride salt (0.85 g, 40% yield).^{1}H NMR (D_2O, 300 MHz): δ_H 8.57 (s, 1H), 8.23 (d, J = 9 Hz, 2H), 8.08 (d, J = 9 Hz, 2H), 7.96 (t, J = 8 Hz, 1H), 7.71 (t, J = 8 Hz, 2H), 7.59 (t, J = 8 Hz, 2H), 7.45 (d, J = 8 Hz, 2H), 5.19 (s, 2H), 4.61 (s, 4H), 3.48 (t, J = 6 Hz, 2H), 3.23 (m, 4H), 3.04 (t, J = 6 Hz, 2H) 2.88 (t, J = 5 Hz, 4H). ^{13}C NMR (D_2O, 75.43 MHz): δ_C 131.1, 130.5, 129.7, 128.1, 125.8, 122.8, 122.4, 120.7, 50.9, 50.6, 49.7, 46.1, 43.3, 40.1. Anal. Calcd for $C_{28}H_{33}N_5{\cdot}4HCl{\cdot}2H_2O$: C, 54.1; H, 6.6; N, 11.3. Found: C, 53.9; H, 6.8; N, 11.2.

*6-(6-Amino-3-azahexyl)-3,6,9-triaza-1-(2,6)-pyridinecyclodecaphane (**L4**).* Pertosylated compound **L6** (2.59 g, 3.64 mmol) was disolved in acetonitrile (250 mL) along with *N*-(3-bromopropyl)-phthalimide (1.19 g, 4.14 mmol) and K_2CO_3 (1.51 g, 10.93 mmol). A white compound was obtained and then washed in ethanol and dried in vacuum (2.75 g, 3.57 mmol, 98%). ^{1}H NMR ($CDCl_3$, 300.13 MHz): δ_H 7.79 (m, 9H), 7.34 (m, 10H), 4.34 (s, 4H), 3.71 (t, 2H), 3.15(m, 6H), 2.99 (t, 2H), 2.63 (t, 2H), 2.44−2.37 (m, 11H), 1.88 (q, 2H). The product obtained in the previous reaction was dissolved in warm dry ethanol along with N_2H_4 (1.12 g, 35 mmol) under reflux for 2 h. A white solid appeared and was removed by filtration. The solvent was evapored, and a yellow oil was obtained. ^{1}H NMR ($CDCl_3$, 300.13 MHz): δ_H 7.66 (m, 7H), 7.23 (m, 8H), 4.30 (s, 4H), 3.10−2.96 (m, 8H), 2.70 (t, 2H), 2.52 (t, 2H), 2.42−2.33 (m 12H), 1.63 (q 2H). ^{13}C NMR ($CDCl_3$, 75.47 MHz): δ_C 155.16, 143.81, 143.50, 138.92, 136.44, 135.99, 130.12, 130.00, 127.43, 127.39, 124.13, 54.72, 51.89, 47.26, 47.18, 44.73, 38.98, 32.15, 21.75, 21.71. This yellow oil was dissolved in HBr in 33% acetic acid (40 mL) and phenol (4 g, 43 mmol) under reflux. After 24 h, a white powder was obtained and subsequently washed in ethanol and dried. The final product was the hydrobromide salt of **L4**. ^{1}H NMR (D_2O, 300.13 MHz): δ_H 8.01 (t, J = 7.82 Hz, 1H), 7.50 (d, J = 7.82 Hz, 2H), 4.69 (s, 4H), 3.34 (m, 6H), 3.14 (m, 4H), 2.98 (m, 2H), 2.16 (m, 2H). ^{13}C NMR (D_2O, 75.47 MHz): δ_C 140.07, 122.50, 149.15, 49.75, 50.83, 46.20, 45.37, 51.22, 43.66, 24.16, 36.84.

This scorpiand ligand was conveniently used as a precursor in the syntheses of **L2** and **L3**.

*6-[8-(9-Anthryl)-3,7-diazaoctyl]-3,6,9-triaza-1-(2,6)-pyridinecyclodecaphane (**L2**).* **L4** (0.42 g, 1.4 mmol) was dissolved in dry ethanol (150 mL), and a solution of 100 mL of dry ethanol containing anthracene-9-carboxaldehyde (0.3 g, 1.4 mmol) was added dropwise. The mixture was then stirred for 2 h. $NaBH_4$ (0.5 g, 14 mmol) was added, and the resulting solution was stirred for 1 h at room temperature. The solvent was evaporated under reduced pressure, and the resulting residue was treated with H_2O. The product was repeatedly extracted with dichloromethane (3 × 30 mL). The organic phase was dried (Na_2SO_4) and evaporated to yield the free amine, which was dissolved in ethanol and precipitated as the hydrochloride salt (0.66 g, 65% yield). ^{1}H NMR (D_2O, 300 MHz): δ_H 8.46 (s, 1H), 8.11 (d, J = 9 Hz, 2H), 8.02 (t, J = 8 Hz, 2H), 7.98 (d, J = 8 Hz, 1H), 7.69 (t, J = 7 Hz, 2H), 7.58 (t, J = 7 Hz, 2H), 7.48 (d, J = 8 Hz, 2H), 5.04 (s, 2H), 4.64 (s, 4H), 3.28 (m, 8H), 3.17 (t, J = 7 Hz, 2H), 3.05 (t, J = 7 Hz, 2H), 2.92 (t, J = 5 Hz, 4H), 2.16 (m, 2H). ^{13}C NMR (D_2O, 75.43 MHz): δ_C 140.2, 131.1, 130.6, 129.8, 128.1, 125.9, 122.8, 122.5, 120.6, 66.9, 51.2, 50.8, 49.8, 46.2, 45.3, 45.0, 43.8, 43.3, 23.1. Anal. Calcd for $C_{31}H_{40}N_6{\cdot}5HCl{\cdot}2H_2O$: C, 52.1; H, 6.9; N, 11.8. Found: C, 52.2; H, 7.0; N, 11.3.

*6-[8-(1-Pyrenyl)-3,7-diazaoctyl]-3,6,9-triaza-1-(2,6)-pyridinecyclodecaphane (**L3**).* **L4** (0.48 g, 1.6 mmol) was dissolved in dry ethanol (150 mL), and a solution of 100 mL of dry ethanol containing pyrene-1-carboxaldehyde (0.36 g, 1.6 mmol) was added dropwise to the former solution. The mixture was then stirred for 2 h. $NaBH_4$ (0.6 g, 16 mmol) was added, and the resulting solution was stirred for 1 h at room temperature. The solvent was evaporated under reduced pressure, and the resulting residue was treated with H_2O. The product was repeatedly extracted with dichloromethane (3 × 30 mL). The organic phase was dried (Na_2SO_4) and evaporated to yield the free amine, which was dissolved in ethanol and precipitated as the hydrochloride salt (0.28 g, 27% yield). ^{1}H NMR (D_2O, 300 MHz): δ_H 7.98 (t, J = 8 Hz, 2H), 7.86 (m, 2H), 7.78 (d, J = 9 Hz, 1H), 7.75 (d, J = 3 Hz, 1H), 7.72 (d, J = 2 Hz, 1H), 7.66 (d, J = 9 Hz, 1H), 7.61 (d, J = 9 Hz, 1H), 7.31 (d, J = 8 Hz, 2H), 4.49 (s, 2H), 4.45 (s, 4H), 3.05 (m, 8H), 2.85 (m, 4H), 1.97 (m, 2H). ^{13}C NMR (D_2O, 75.43 MHz): δ_C 149.1, 140.1, 131.8, 130.8, 130.1, 128.8, 128.7, 128.6, 128.4, 127.3, 126.7, 126.2, 126.1, 125.0, 123.6, 123.3, 122.4, 121.48, 51.0, 50.5, 49.8, 46.1, 44.4, 43.5, 23.0. Anal. Calcd for $C_{33}H_{40}N_6{\cdot}4HCl{\cdot}3H_2O$: C, 55.0; H, 7.0; N, 11.7. Found: C, 54.9; H, 6.9; N, 11.8.

Electromotive Force Measurements. The potentiometric titrations were carried out in water at 298.1 ± 0.1 K using 0.15 mol dm^{-3} NaCl as the supporting electrolyte. NaCl was chosen as the inert electrolyte because of both the higher solubility of the receptor in this medium and the high content of this salt in extracellular fluids. The experimental procedure (buret, potentiometer, cell, stirrer, microcomputer, etc.) has been fully described elsewhere.[34] The acquisition of the emf data was performed with the computer program PASAT.[35]The reference electrode was an Ag/AgCl electrode in saturated KCl solution. The glass electrode was calibrated as an hydrogen ion concentration probe by titration of previously standardized amounts of HCl with CO_2-free NaOH solutions and determination of the equivalence point by the Grańs method,[36] which gives the standard potential, $E^{\circ\prime}$, and the ion product obtained was 13.73(1) in pure water.[37] The computer program HYPERQUAD was used to calculate the protonation and stability constants.[38] The pH range investigated (pH = $-\log[H^+]$) was 2.0−11.0. The different titration curves for each ligand were treated as separate curves without significant variations in the values of the stability constants. Finally, the sets of data were merged together and treated simultaneously to give the final stability constants.

NMR Measurements. NMR samples were prepared under an argon atmosphere in D_2O (99.9%). Adjustments to the desired pD were made using drops of DCl or NaOD solutions. All chemicals were of analytical grade and used without further purification. The pD was calculated from the measured pH values using the correlation pH = pD − 0.4.[39] The NMR spectra were recorded at 298 K using a NMR spectrometer apparatus operating at 300 MHz for ^{1}H and at 75.43 MHz for ^{13}C. Spectra were obtained using a 5 mm inverse broadband probe head incorporating a shielded *Z*-gradient coil. The chemical shifts are given in parts per million referenced to the solvent signal.

X-ray Diffraction Experiments. Slow evaporation of an aqueous solution of **L1** or **L4** along with $Cu(ClO_4)_2$ at pH ∼9 yielded crystals suitable for X-ray diffraction. One single crystal of $[Cu(\mathbf{L1})](ClO_4)_2$ was measured in an Oxford Diffraction Supernova diffractometer using

dx.doi.org/10.1021/ja300538s | *J. Am. Chem. Soc.* 2012, 134, 9644−9656

Mo Kα radiation (λ = 0.71073 Å) at 120 K. One single crystal of $[Cu(\mathbf{L4})](ClO_4)_2$ was measured in an Enraf Nonius Kappa CCD diffractometer using Mo Kα radiation (λ = 0.71073 Å) at room temperature. The structure was solved with the SHELXS-97 program and further refined with SHELXL-97 up to the final structure.[40] Final drawings of the structures were made with the Mercury program.[41]

Spectrofluorimetric Measurements. Double-stranded ctDNA was purchased from commercial sources and used without further purification. The DNA concentration per nucleotide was determined by absorption spectroscopy, using the molar extinction coefficient of 6600 M^{-1} cm^{-1} at 260 nm. Titration experiments were carried out at room temperature by adding increasing amounts of ctDNA to a 5×10^{-5} M ligand solution. All solutions were prepared in 50 mM sodium cacodylate buffer (pH 7.0) using doubly distilled water and passed through a Millipore apparatus. The pH values were measured with a pH meter, and adjustments of the hydrogen ion concentration of the solutions were made with diluted HCl and NaOH solutions. UV−vis absorption spectra were recorded on a spectroscopy system. The computer program HypSpec was used to calculate stability constant values from spectroscopic data.[38] The absorbances of aqueous solutions of all compounds were proportional to their concentrations up to 100 μM. Hence, no significant intermolecular aggregation of the compounds, which would be expected to give rise to hypochromicity effects, occurred in the concentration range needed for the following spectroscopic studies. The emission spectra were recorded with a spectrofluorimeter in the 300−550 nm range with excitation wavelengths of 365 nm for **L1** and **L2** and 341 nm for **L3**. Absorption and volume correction procedures were applied to the raw fluorescence data.

Circular Dichroism Experiments. CD spectra were recorded on a spectropolarimeter between 400 and 200 nm in continuous scanning mode (50 nm/min, 1 nm bandwidth, and 1 s response time). All of the CD spectra were generated and represented averages of three scans. Experiments were performed by adding progressively increasing amounts of ligand to different solutions of ctDNA [$(1-3) \times 10^{-5}$ M] in 50 mM cacodylate buffer (pH 7).

DNA Melting Experiments. Thermal melting curves were measured on an Agilent 8453 spectrometer equipped with a Peltier temperature controller system (±0.1 °C). The ratio of DNA to compound was 2:1. Thermal melting curves for DNA were determined by following the absorption change at 260 nm in 50 mM cacodylate buffer (pH 7.0) in the absence or presence of scorpiand derivatives as a function of temperature. The absorbance of the ligand was subtracted from every curve, and the absorbance scale was normalized. The T_m values were taken as the midpoints of the transition curves, as determined from the maximum of the first derivative and checked graphically by the tangent method. ΔT_m values were calculated subtracting T_m for the free nucleic acid from T_m for the complex.[42] Every ΔT_m value reported here was the average of at least two measurements; the error in ΔT_m was ±0.5 °C.

Ethidium Bromide Displacement Assays. Displacement experiments were recorded on a spectrofluorimeter in the 540−680 nm range with an excitation wavelength of 520 nm. The fluorescence was normalized by the maximum fluorescence signal when EB was bound to the DNA in the absence of competition for binding and was corrected for background fluorescence of free EB in solution.

Viscosity Experiments. Viscosity experiments used an Ubbelohde-type viscometer immersed in a thermostatted water bath maintained at a constant temperature of 25 °C. Solutions were prepared at different ligand concentrations (0, 1, 3, 5, 7, and 10 μM) in 50 mM cacodylate buffer (pH 7.0), keeping the ctDNA concentration constant at 50 μM. Elution times were recorded three times for each of the solutions prepared. Results were plotted as $(\eta/\eta_0)^{1/3}$ versus the binding ratio r, according to the theory of Cohen and Eisenberg.[43]

Cell Cultures. Human bladder carcinoma cell lines (T24, 253J, and UMUC-3) were obtained from the American Type Culture Collection (Rockville, MD). Cells were cultured as monolayers at 37 °C in a humidified 5% CO_2 atmosphere. Cell lines T24 and 253J were maintained in McCoys's 5A medium and UMUC-3 in Dulbecco's modified Eagle's medium plus glutamine; both media were supplemented with 10% heat-inactivated fetal bovine serum, penicillin (100 units/mL), streptomycin (100 mg/L), and amphotericin B (25 μg/L). Cells were routinely detached with trypsin EDTA and subcultured before reaching confluence.

For image analysis, UMUC-3 cells were cultured in a eight-well chamber slide for 24 h and then treated with **L2** or $[Zn(\mathbf{L2})]^{2+}$ at 5 or 10 μM for 16 h and washed twice with phosphate-buffered saline before the fluorescence images were captured.

For immunoblot analysis, UMUC-3 cells were treated for 16 h with 100 nM doxorubicin, 100 μM 5-fluorouracil, **L2**, or $[Zn(\mathbf{L2})]^{2+}$ at concentrations of 6 and 8 μM.

Cell Viability Assays. Cell viability was determined with the 3-(4,5-dimethylthiazol-2-yl-2,5-diphenyltetrazolium bromide (MTT) assay.[44,45] MTT is reduced by the mitochondrial reductase enzymes of living cells to give formazan, which can be directly related to the number of viable (living) cells.[44]

T24, 253J, or UMUC-3 cells [$(3-5) \times 10^3$ cells in 200 μL of the corresponding medium] were seeded in 96-well culture plates and allowed to attach and recover from trypsinization for 24 h. The medium was removed, and the compounds were added to the cells in 0.2 mL of medium. After 24, 48, or 72 h of incubation with the compounds, the cells were incubated for an additional 3 h in fresh medium without compounds but containing 1.2 μmol L^{-1} of MTT. The formazan precipitate was dissolved in 200 μL of dimethyl sulfoxide, and its absorbance was measured at 540 nm using an automatic multiwell spectrophotometer. The rate of survival was calculated as follows: rate of survival (in %) = (1 − OD of experimental well/OD of positive-control well) × 100%. The IC_{50} is defined as the concentration of a compound that causes a 50% reduction in cell viability relative to untreated controls. IC_{50} values were calculated using nonlinear regression analysis dose−response curve fitting.

Image Analysis. Fluorescence images were obtained with a Nikon fluorescence microscope (TE2000-E) using the NIS-Elements Nikon software and processed using the MacBiophotonics ImageJ 1.43 m software.

Immunoblotting. After the different treatments, cell lysates were prepared as described elsewhere.[46] The lysates (30 μg of total protein) were resolved by 10% sodium dodecyl sulfate polyacrylamide gel electrophoresis and transferred onto nitrocellulose membranes. The membranes were incubated with anti-p53 (pSer15) (Ab-3) rabbit polyclonal antibody (1:1000 dilution, overnight at 4 °C), anti-p53 Ab-1 (Oncogene Research Products) (1:500 dilution, 2 h at room temperature), and anti-β-actin (Clone AC-74) (1:5000 dilution, 1 h at room temperature). The secondary antibody incubation and detection by chemiluminescence were performed as detailed elsewhere.[46]

p53 and pSer15-p53 protein expression were quantified by densitometry using Quantity One software (Bio-Rad). The phosphorylation fold increases were calculated as the ratios of pSer15-p53/p53 protein expression and plotted as percentages of the controls.

■ ASSOCIATED CONTENT

Ⓢ Supporting Information

Steady-state fluorescence emission titration curves, ^1H NMR spectra, absorption spectra, plot of percent hypochromism versus base pair/complex, CD fluorescence spectra, cell viability information, and crystallographic data (CIF). This material is available free of charge via the Internet at http://pubs.acs.org.

■ AUTHOR INFORMATION

Corresponding Author

teresa.albelda@uv.es; agarciae.hj23.ics@gencat.cat; enrique.garcia-es@uv.es

Present Address

[‖]Department of Biomedical Sciences, University CEU Cardenal Herrera, C/Grecia 31, 12006 Castellón de la Plana, Castellón, Spain

Notes

The authors declare no competing financial interest.

■ ACKNOWLEDGMENTS

We thank MICINN (Spain) for financial support (Projects CONSOLIDER INGENIO CSD-2010- 00065 and CTQ2009-14288-C04-01) and GVA (Project PROMETEO 2011/008). A.G.-E. was supported by the Research Stabilization Program of the Instituto de Salud Carlos III-Institut Catala de la Salut in Catalonia. M.T.A. thanks Ajuntament de València for her "Carmen y Severo Ochoa" Grant. B.V. thanks MICINN for a Juan de la Cierva Grant.

■ REFERENCES

(1) Chenoweth, D. M.; Dervan, P. B. *Proc. Natl. Acad. Sci. U.S.A.* **2009**, *106*, 13175−13179.
(2) (a) Chaires, J. B. Energetics of Anthracycline−DNA Interactions. In *Small Molecule DNA and RNA Binders: From Synthesis to Nucleic Acid Complexes*; Demeunynck, M., Bailly, C., Wilson, W. D., Eds; Wiley-VCH: Weinheim, Germany, 2004; Chapter 17. (b) Gurova, K. *Future Oncol.* **2009**, *5*, 1685−1704.
(3) Liu, Y; Wilson, W. D. *Methods Mol. Biol.* **2010**, *613*, 1−23.
(4) Havelka, A. M.; Berndtsson, M.; Olofsson, M. H.; Shoshan, M. C.; Linder, S. *Mini-Rev. Med. Chem.* **2007**, *7*, 1035−1039.
(5) (a) Hannon, M. J. *Chem. Soc. Rev.* **2007**, *36*, 280−295. (b) Long, E. C.; Barton, J. K. *Acc. Chem. Res.* **1990**, *23*, 271−273.
(6) Kim, R. *Cancer* **2005**, *103*, 1551−1560.
(7) (a) Liu, H. K.; Sadler, P. J. *Acc. Chem. Res.* **2011**, *44*, 349−359. (b) Lenglet, G.; David-Cordonnier, M.-H. *J. Nucleic Acids* **2010**, No. 290935. (c) Hendry, L. B.; Mahesh, V. B.; Bransome, E. D., Jr.; Ewing, D. E. *Mutat. Res., Fundam. Mol. Mech. Mutagen.* **2007**, *623*, 53−71.
(8) (a) Liang, F.; Wan, S.; Li, Z.; Xiong, X.; Yang, L.; Zhou, X.; Wu, C. *Curr. Med. Chem.* **2006**, *13*, 711−727. (b) Granzhan, A.; Largy, E.; Saettel, N.; Teulade-Fichou, M. P. *Chem.—Eur. J.* **2010**, *16*, 878−889. (c) Chand, D. K.; Schneider, H.-J.; Aguilar, J. A.; Escartí, F.; García-España, E.; Luis, S. V. *Inorg. Chim. Acta* **2001**, *316*, 71−78.
(9) (a) Lotz, T. J.; Kaden, T. A. *J. Chem. Soc., Chem. Commun.* **1977**, 15−16. (b) Pallavicini, P. S.; Perotti, A.; Poggi, A.; Segui, B.; Fabbrizzi, L. *J. Am. Chem. Soc.* **1987**, *109*, 5139−5144.
(10) Verdejo, B.; Ferrer, A.; Blasco, S.; Castillo, C. E.; González, J.; Latorre, J.; Máñez, M. A.; Basallote, M. G.; Soriano, C.; García-España, E. *Inorg. Chem.* **2007**, *46*, 5707−5719.
(11) (a) Ikeda, T.; Yoshida, K.; Schneider, H.-J. *J. Am. Chem. Soc.* **1995**, *117*, 1453−1454. (b) Lomadze, N.; Gogritchiani, E.; Schneider, H.-J.; Albelda, M. T.; Aguilar, J.; García-España, E.; Luis, S. V. *Tetrahedron Lett.* **2002**, *43*, 7801−7803. (c) Malojcic, G.; Piantanida, I.; Marinic, M.; Zinic, M.; Marjanovic, M.; Kralj, M.; Pavelic, K.; Schneider, H.-J. *Org. Biomol. Chem.* **2005**, *3*, 4373−4381. (d) Lomadze, N.; Schneider, H.-J.; Albelda, M. T.; García-España, E.; Verdejo, B. *Org. Biomol. Chem.* **2006**, *4*, 1755−1759.
(12) (a) Sarnesky, J. E.; Surprenant, H. L.; Molen, F. K.; Reiley, C. N. *Anal. Chem.* **1975**, *47*, 2116−2124. (b) Bencini, A.; Bianchi, A.; García-España, E.; Micheloni, M.; Ramírez, J. A. *Coord. Chem. Rev.* **1999**, *188*, 97−156.
(13) (a) Albelda, M. T.; García-España, E.; Jiménez, H. R.; Llinares, J. M.; Soriano, C.; Sornosa-Ten, A.; Verdejo, B. *Dalton Trans.* **2006**, 4474−4481. (b) Frassineti, C.; Ghelli, S.; Gans, P.; Sabatini, A.; Moruzzi, M. S.; Vacca, A. *Anal. Biochem.* **1995**, *231*, 374−382. (c) Frassineti, C.; Alderighi, L.; Gans, P.; Sabatini, A.; Vacca, A.; Ghelli, S. *Anal. Bioanal. Chem.* **2003**, *376*, 1041−1052.
(14) (a) Dagnall, S. P.; Hague, D. N.; McAdam, M. E.; Moreton, A. D. *J. Chem. Soc., Faraday Trans. 1* **1985**, *81*, 1483−1494. (b) Hague, D. N.; Moreton, A. D. *J. Chem. Soc., Perkin Trans. 2* **1994**, 265−270.
(15) (a) Julliard, M.; Chanon, M. *Chem. Rev.* **1983**, *83*, 425−506. (b) de Silva, A. P.; Dayasiri Rupasinghe, R. A. D. *J. Chem. Soc., Chem. Commun.* **1985**, 1669−1670.
(16) Zhang, S.-C.; Tu, C.; Wang, X.-Y.; Yang, Z.; Zhang, J.-Y.; Lin, L.-P.; Ding, J.; Guo, Z.-J. *Eur. J. Inorg. Chem.* **2004**, 4028−4035.
(17) Sheng, X.; Lu, X.-M.; Chen, Y.-T.; Lu, G.-Y.; Zhang, J.-J.; Shao, Y.; Liu, F.; Qiang, X. *Chem.—Eur. J.* **2007**, *13*, 9703−9712.
(18) (a) de Silva, A. P.; Gunaratne, H. Q. N.; Gunnlaugsson, T.; Huxley, A. J. M.; McCoy, C. P.; Rademacher, J. T.; Rice, T. E. *Chem. Rev.* **1997**, *97*, 1515−1566. (b) de Silva, A. P.; Gunaratne, H. Q. N.; McCoy, C. P. *Chem. Commun.* **1996**, 2399−2400.
(19) Addison, A. W.; Rao, T. N.; Reedijk, J.; van Rijn, J.; Verschoor, G. C. *J. Chem. Soc., Dalton Trans.* **1984**, 1349−1356.
(20) Pyle, A. M.; Rehmann, J. P.; Meshoyrer, R.; Kumar, C. V.; Turro, N. J.; Barton, J. K. *J. Am. Chem. Soc.* **1989**, *111*, 3051−3058.
(21) Long, E. C.; Barton, J. K. *Acc. Chem. Res.* **1990**, *23*, 271−273.
(22) Tan, W. B.; Bhambhani, A.; Duff, M. R.; Rodger, A.; Kumar, C. V. *Photochem. Photobiol.* **2006**, *82*, 20−30.
(23) Speciation studies indicated the following speciation for the Cu^{2+}−**L** and Zn^{2+}−**L** systems at pH 7 with reactant concentrations of 10^{-3} mol L^{-1}: Cu^{2+}−**L1**, 100% $[Cu(\mathbf{L1})]^{2+}$; Zn^{2+}−**L1**, 100% $[Zn(\mathbf{L1})]^{2+}$; Cu^{2+}−**L2**, 80% $[Cu(\mathbf{L2})]^{2+}$, 20% $[Cu(\mathbf{HL2})]^{3+}$; Zn^{2+}−**L2**, 67% $[Zn(\mathbf{L2})]^{2+}$, 33% $[Zn(\mathbf{HL2})]^{3+}$; Cu^{2+}−**L3**, 88% $[Cu(\mathbf{L3})]^{2+}$, 12% $[Cu(\mathbf{HL3})]^{3+}$; Zn^{2+}−**L3**, 52% $[Zn(\mathbf{L3})]^{2+}$, 48% $[Zn(\mathbf{HL3})]^{3+}$.
(24) Bush, C. A. In *Basic Principles in Nucleic Acid Chemistry*; Ts'o, P. O. P., Ed.; Academic Press: New York, 1974; Vol. 2, p 102.
(25) (a) Lyng, R.; Härd, T.; Norden, B. *Biopolymers* **1987**, *26*, 1327−1345. (b) Norden, B.; Tjerneld, F. *Biopolymers* **1982**, *21*, 1713−1734. (c) Schipper, P. E.; Norden, B.; Tjerneld, F. *Chem. Phys. Lett.* **1980**, *70*, 17−21.
(26) (a) Modukuru, N. K.; Snow, K. J.; Perrin, B. S., Jr.; Bhambhani, A.; Duff, M.; Kumar, C. V. *J. Photochem. Photobiol., A* **2006**, *177*, 43−54. (b) Duff, M. R.; Tan, W. B.; Bhambhani, A.; Perrin, B. S., Jr.; Thota, J.; Rodger, A.; Kumar, C. V. *J. Phys. Chem. B* **2006**, *110*, 20693−20701. (c) Modukuru, N. K.; Snow, K. J.; Perrin, B. S., Jr.; Thota, J.; Kumar, C. V. *J. Phys. Chem. B* **2005**, *109*, 11810−11818. (d) Rodger, A.; Taylor, S.; Adlam, G.; Blagbrough, I. S.; Haworth, I. S. *Bioorg. Med. Chem.* **1995**, *3*, 861−872.
(27) Haq, I.; Jenkins, T. C.; Chowdhry, B. Z.; Ren, J. S.; Chaires, J. B. *Methods Enzymol.* **2000**, *323*, 373−405.
(28) Kumar, C. V.; Asuncion, E. H. *J. Am. Chem. Soc.* **1993**, *115*, 8547−8553.
(29) Suh, D.; Chaires, J. B. *Bioorg. Med. Chem.* **1995**, *3*, 723−728.
(30) López-Knowles, E.; Hernández, S.; Malats, N.; Kogevinas, M.; Lloreta, J.; Carrato, A.; Tardón, A.; Serra, C.; Real, F. X. *Cancer Res.* **2006**, *66*, 7401−7404.
(31) Sanchez-Carbayo, M.; Socci, N. D.; Charytonowicz, E.; Lu, M. L.; Prystowsky, M.; Childs, G.; Cordon-Cardo, C. *Cancer Res.* **2002**, *62*, 6973−6980.
(32) Shieh, S. Y.; Ikeda, M.; Taya, Y.; Prives, C. *Cell* **1997**, *91*, 325−334.
(33) (a) Verma, R.; Rigatti, M. J.; Belinsky, G. S.; Godman, C. A.; Giardina, C. *Biochem. Pharmacol.* **2010**, *79*, 565−574. (b) Makovski, A.; Yaffe, E.; Shpungin, S.; Nir, U. *Cell. Signalling* **2012**, *24*, 1369−1374.
(34) García-España, E.; Ballester, M. J.; Lloret, F.; Moratal, J. M.; Faus, J.; Bianchi, A. *J. Chem. Soc., Dalton Trans.* **1988**, 101−104.
(35) Fontanelli, M.; Micheloni, M. In *Proceedings of the First Spanish−Italian Congress on Thermodynamics of Metal Complexes*, Diputación de Castellón, Spain, 1990.
(36) (a) Gran, G. *Analyst* **1952**, *77*, 661−671. (b) Rossotti, F. J. C.; Rossotti, H. *J. Chem. Educ.* **1965**, *42*, 375−378.
(37) Avdeef, A.; Box, K. J.; Comer, J. E. A.; Gilges, M.; Hadley, M.; Hibbert, C.; Patterson, W.; Tam, K. Y. *J. Pharm. Biomed. Anal.* **1999**, *20*, 631−641.
(38) Gans, P.; Sabatini, A.; Vacca, A. *Talanta* **1996**, *43*, 1739−1753.
(39) (a) Glasoe, P. K.; Long, F. A. *J. Phys. Chem.* **1960**, *64*, 188−190. (b) Covington, A. K.; Paabo, M.; Robinson, R. A.; Bates, R. G. *Anal. Chem.* **1968**, *40*, 700−706.
(40) Sheldrick, G. M. *Acta Crystallogr.* **2008**, *A64*, 112−122.

(41) Macrae, C. F.; Bruno, I. J.; Chisholm, J. A.; Edgington, P. R.; McCabe, P.; Pidcock, E.; Rodriguez-Monge, L.; Taylor, R.; van de Streek, J.; Wood, P. A. *J. Appl. Crystallogr.* **2008**, *41*, 466−470.
(42) Chaires, J. B.; Dattagupta, N.; Crothers, D. M. *Biochemistry* **1982**, *21*, 3933−3940.
(43) Cohen, G.; Eisenberg, H. *Biopolymers* **1969**, *8*, 45−55.
(44) Mosmann, T. *J. Immunol. Methods* **1983**, *65*, 55−63.
(45) Alley, M. C.; Scudiero, D. A.; Monks, A.; Hursey, M. L.; Czerwinski, M. J.; Fine, D. L.; Abbott, B. J.; Mayo, J. G.; Shoemaker, R. H.; Boyd, M. R. *Cancer Res.* **1988**, *48*, 589−601.
(46) García-España, A.; Salazar, E.; Sun, T. T.; Wu, X. R.; Pellicer, A. *Cancer Res.* **2005**, *65*, 1150−1157.